Macromolecules
ARTICLE

Macromolecules **2009**, *42*, 4751–4757 **4751**
DOI: 10.1021/ma9004567

Shear-Induced Nucleation and Growth of Long Helices in Supercooled Isotactic Polypropylene

Yong Geng,[†,‡] Guanglin Wang,[‡] Yuanhua Cong,[‡] Liangui Bai,[‡] Liangbin Li,*[,‡] and Chuanlu Yang[†]

[†]*Department of Physics and Electrons, Ludong University, Yantai, China, and* [‡]*National Synchrotron Radiation Lab and Department of Polymer Science and Engineering, University of Science and Technology of China, Hefei, China*

Received March 2, 2009; Revised Manuscript Received April 15, 2009

ABSTRACT: Flow-induced conformational ordering in the supercooled isotactic polypropylene (iPP) is studied with in situ Fourier transform infrared spectroscopy (FTIR) coupled to an extrusion slit die. At temperature around the normal melting point of iPP, helices with monomer numbers up to 12 and 14 can be induced by shear. A window of shear strength exists to induce helices with different lengths, which increases with temperature. After the cessation of shear, the intensity of the 841 cm^{-1} band in FTIR spectra, corresponding to helices with 12 monomers, increases sharply in the first stage, which is followed by a slow growth process, whereas a reduction of shorter helices is observed after the cessation of shear. The different trends of intensity evolutions of the long and short helical bands suggest that a coupling between coil−helix transition and intermolecular ordering occurs with helices with a length of 12 monomers, which eventually leads to an isotropic−liquid-crystal transition. Therefore, the flow-induced precursor may be a liquid crystal phase, which will transform into crystal and initiate crystal growth later.

Introduction

Polymer rheology and flow-induced ordering are two essential aspects that control polymer processing and are also the core of polymer physics.[1−4] A great deal of effort has been devoted to studying flow-induced crystallization of polymers since the middle of the last century.[5−18] In particular, during the past decade, some new observations and insights were drawn out through experiment methods such as X-ray and neutron scattering[19−24] and computer simulation.[10,13,25] A well-accepted preordering or precursors induced by shearing was reported, which holds the key to establish the molecular mechanism of flow-induced crystallization of polymer.[26−28] The evidence of the preordering is mainly from the equatorial scattering of small-angle X-ray or neutron scattering measurements, which give two long streaks close to the beam stop.[29−31] Because these streaks appear well before the crystalline diffraction peaks in the wide angle scattering region, the preordering is recognized to be noncrystalline. On the basis of the scattering evidence, a conclusion that density fluctuation is induced by shear can be drawn. In the search for the role of long and short chains during flow-induced crystallization, mixtures of polymers with different chain lengths are widely employed as a model system for the study.[32−34] This, however, may bring in complications such as concentration fluctuation or phase separation, which can give similar scattering patterns at equatorial position.[35−37] Flow-induced orientational ordering is also a reasonable consequence, which is supported not only by scattering data but also by birefringence and depolarized light scattering measurements.[38,39] Furthermore, shear-induced all-trans sequences with a lifetime of several hours were found in the rheo-Raman experiments, which enlightens the occurrence of conformational ordering.[40] An indirect but strong evidence of precursor was reported by the Alfonso group, who derived the lifetime of the flow-induced precursor through the influence on subsequent crystallization behavior after waiting different relaxation time.[41,42] A summary of the reported experimental evidence suggests that the flow-induced precursor is oriented nanobundles possibly with a higher density or concentration than the initial melt under quiescent conditions. Nevertheless, detailed structure information inside the bundles is still absent, which keeps the concept of precursor to be somehow rather vague.

Crystallization of polymer comprises intermolecular and intramolecular ordering.[43,44] Intermolecular ordering includes position and orientational ordering, whereas intramolecular ordering is mainly conformational ordering, which is unique for polymer. Therefore, the preordering or precursor induced by flow should contain only some of these orderings but not all of them. Compared with intermolecular ordering, intramolecular ordering received less attention possibly because of technical limitation, although many studies were reported under quiescent conditions.[45−47] Following an intuitive picture of the flow-induced crystallization process, imposing flow field on polymer chains should first lead the individual molecular chain to be either oriented or stretched, which is accompanied by intramolecular ordering such as conformational ordering or coil−helix transition.[48−50] Then, the second step can be the packing process of neighboring chains, which is the intermolecular ordering process. Therefore, the intuitive picture tells us that understanding flow-induced conformational ordering may be the first step to unveiling the full scene of flow-induced crystallization of polymer.

Middle infrared (IR) bands are mainly vibrational bands whose direct origin is the existence of the dipole moment. As discussed in refs 51and 52, the finite helical length and the interaction between adjacent monomers lead a single vibration mode to splitting into *n* components. Therefore, although the vibrational modes are the same, different helical length and local environment can result in absorption bands at different wave numbers, as revealed by calculations and experiments of Snyder et al.[53] and Zhu et al.[54] For example, 841, 998, and 973 cm^{-1}

*Corresponding author. E-mail: lbli@ustc.edu.cn.

Published on Web 05/21/2009

Table 1. Infrared Bands versus Helical Length

wave number (cm^{-1})	vibrational mode(s)	corresponding number of monomers in helices
973	C−C stretching; CH_2 rocking; CH_3 rocking	3 to 4
808	C−C stretching; coupled C−H deformation	~7
841	C−C stretching; CH_2 rocking; CH_3 rocking	12
900	C−C stretching; coupled C−H deformation	~8
940	C−C stretching; coupled C−H deformation	> 14
998	C−C stretching; CH_2 rocking; CH_3 rocking	10
1100	C−CH_3 stretching; CH_3 rocking; CH bending	~6
1167	C−C stretching; CH_3 wagging	~6
1220	CH_2 twisting; CH bending; C−CH_3 stretching	14
1303	C−H bending	~13
1330	CH bending; CH_2 twisting	~13

bands of isotactic polypropylene (iPP) correspond to helical lengths with monomers of 14, 10, and 3 to 4, respectively.[54] Focusing on conformational ordering, we have recently studied shear-induced coil−helix transition in iPP.[55,56] Because different helical lengths show different IR absorption bands (Table 1), it is convenient to follow the shear effect on the content and the length of helices.[53−63] Zhu et al. found that conformational bands such as 973, 1100, 808, and 900 cm^{-1} are present at high temperature, whereas the 841 cm^{-1} band would not appear until a temperature of about 120 °C. As soon as the 841 cm^{-1} band appears, 1330, 1303, 1167, 1220, and 940 cm^{-1} bands emerge, and the intensities of all conformational bands increase, which indicates the occurrence of crystallization, as confirmed by their DSC data.[62] Therefore, by comparing the intensity evolution of all conformational bands, the onset of crystallization can be conveniently justified. As mentioned before, iPP melt helices with monomer numbers up to 10 (998 cm^{-1}) already exist. By monitoring the intensity evolution of 998 and 1100 cm^{-1} bands, we observed that shear induces an increase in helical length and content at temperatures higher than the melting temperature (165 °C). Here the increase in helical length is from shorter ones to a helix with monomer number of 10 (998 cm^{-1}), but our previous work did not observe helices with a larger monomer number before crystallization.

Without crystallization, can helices with a monomer number larger than 10 be induced by shear? This question is critical to verify shear-induced nucleation and growth of long helices and ultimately leads to crystallization. To answer this question, iPP is an ideal material to test this question. In an IR spectrum of iPP, the 841 cm^{-1} band corresponds to helical length with 12 monomers, which is not observed in the melt under quiescent conditions. Therefore, by simply checking the appearance of the 841 cm^{-1} band after imposing shear, we can justify whether shear leads to the formation of long helices. However, following the intensity evolution of all conformational bands, the onset of crystallization can be verified. In this work, 1100, 998, 841, and 1220 cm^{-1} bands were simultaneously monitored, which allows us to judge whether long helices can be induced by shear without the occurrence of crystallization. Additionally, we also check whether the 1220 cm^{-1} band appears or not. The appearance of the 1220 cm^{-1} band may not represent the onset of crystallization, but without the 1220 cm^{-1} band, crystallization definitely does not occur.

On the basis of our previous work, three improvements or extensions were made in this work. (i) A new shearing cell was designed to minimize sample thickness fluctuation before and after the shear, which will be described in the Experimental Section. (ii) The experimental temperatures were chosen to be close to or lower than melting temperature, which created the possibility for long helices to appear. (iii) We used differential spectra to analyze the data, which enhanced the quality of the data and provided more direct information. Our results indicated that helices with 12 monomers can be induced with shear field. The stability of the long helices is attributed to the coupling between intramolecular and intermolecular ordering, which leads to the conclusion that the shear-induced precursor may be a liquid crystalline phase.

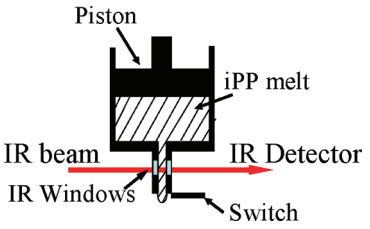

Figure 1. Schematic picture of the homemade shear flow instrument.

Experimental Section

The iPP used in this study was F401, a commercial product of Lanzhou Petroleum Chemical (China) that has M_w and M_n values of about 530 and 160 kg/mol, respectively, and whose tacticity is 97%.

An instrument driven by a servomotor has been constructed to provide the shear flow, which is a mini extruder and schematically illustrated in Figure 1. The mechanism of shear is similar to those from Kornfield[11] and Janeschitz-Kriegl.[5] The shear-flow instrument has a reservoir that is used to store the iPP melt. A slit die is designed to impose the shear on the melt. The length of the slit along the flow direction is 15 mm, and the cross section has a dimension width × height of 13 × 0.5 mm^2. Two ZnSe windows for IR beam are fixed on the steel die with a gap the same as the height of slit (0.5 mm). A parabolic flow profile is distributed in the shearing gap. By controlling the servomotor speed and the detecting point along the length direction, it is possible to tune the shear rate and strain, respectively. In this work, we fixed the detecting point at the middle of the length (7.5 mm) and only changed the motor speed. The servomotor is controlled by software compiled with Labview.

During experiments, the sample was first heated to 220 °C for 10 min to erase possible memory effects. Then, it was cooled to the required temperature, T_s, and held for 10 min before the shear was imposed. Starting the servomotor with a certain rate, the piston would go ahead to extrude the iPP melt out of the slit. When the extruded melt flow was stabilized, the motor was stopped and the switch was turned on simultaneously, which prevented the iPP melt from flowing out continuously. The flow rates used in this study were 4.5, 9, 18, 45, 75, 90, and 180 mm^3/s.

In situ IR spectra were collected over a wavenumber range of 700−2000 cm^{-1} using a Bruker Tensor 37 FTIR spectrometer with a resolution of 2 cm^{-1}. All of the IR measurements were taken at the same temperature when imposing shear flow. Differential spectra were used to analyze the data, where all spectra subtracted the one before shear. The integrated peak intensity was used to follow the content of helices.

Results

Before putting our focus on the precursor, we first check the intensity evolution of the conformational bands during crystallization with and without imposing shear, respectively. Figure 2 a shows the intensity evolution of 1100, 998, 841, and 1220 cm^{-1} bands of iPP sample at 142 °C, whereas the intensity evolution of the same bands at 145 °C after imposing a shear with a flow rate

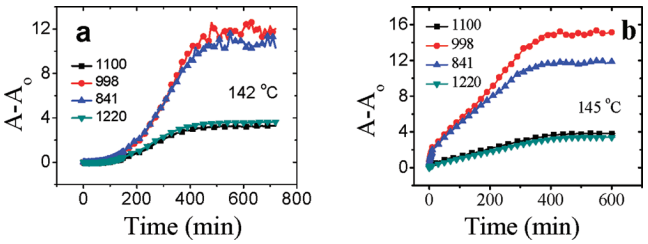

Figure 2. IR intensity evolution of 1220, 1100, 998, and 841 cm^{-1} bands of iPP (a) at 142 °C without shear and (b) after shear at 145 °C, respectively.

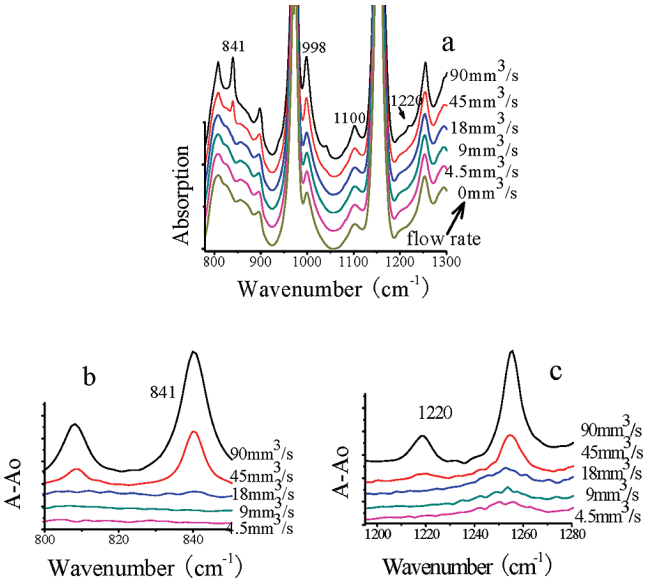

Figure 3. (a) Spectra before and just after the cessation of shear with different shear flow rates at 150 °C. (b,c) Corresponding differential spectra in the regions of 750−900, 985−1090, and 1175−1230 cm^{-1}, respectively.

of 18 mm^3/s is presented in Figure 2 b. A slightly higher temperature for shearing experiment is to ensure reasonable crystallization kinetics for IR to record. Under quiescent conditions, it takes about 100 min for crystallization to start at 142 °C, where all conformational bands increase intensity during the crystallization process.[62] However, the imposing of shear flow leads to a sharp increase, and all conformational bands increase without any relaxation process, which indicates that crystallization occurs immediately after shear. The first sharp increase in intensity due to the effect of shear may represent the fact that crystalline precursor is brought in by shear, as reported by Balzano et al.[64]

Figure 3a gives the representative original IR spectra date before and just after shear at 150 °C under different shear flow rates, which were carefully baseline adjusted at a uniform standard. It clearly shows that the shear flow induced a sharp increase in the intensity of the conformational ordering bands. The increase in the IR intensities is mainly attributed to the increase in helical populations rather than helical orientation because the conformational bands with a polarization direction parallel and perpendicular to the helix axis all show an increase in intensity after shear. The orientation of helices induced by shear certainly contributes to the intensity evolution. However, with an unpolarized beam and detection system, the orientational effect is a minor factor and does not affect the result in this study. Moreover, 841 and 1220 cm^{-1} bands do not appear in the melt under quiescent conditions; the occurrence of those bands after shear is certainly shear-induced rather than being due to

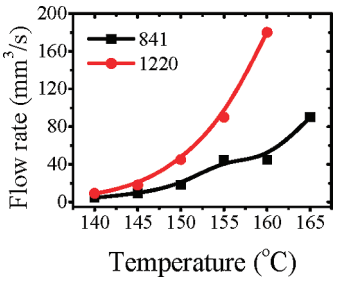

Figure 4. The critical flow rate to induce the appearance of 841 and 1220 cm^{-1} bands at various temperature.

shear-alignment. When the shear-flow rate decreases, the spectra differences become illegible. Differential spectra were introduced to distinguish the small differences, where all spectra after shear subtracted the one before shear. Figure 3b,c shows 841 and 1220 cm^{-1} bands in the differential spectra just after shear with different shearing strength. With a flow rate of 18 mm^3/s, the 841 cm^{-1} band appears immediately after shear, whereas a flow rate of 45 mm^3/s is required to induce the occurrence of the 1220 cm^{-1} band. This difference clearly indicates that a flow rate window exists to induce the formation of these long helices with monomer numbers of 12 and 14.

Following the same experimental procedure as that at 150 °C, we investigated the flow rate window to induce the appearance of 841 and 1220 cm^{-1}. Figure 4 plots the critical flow rates to induce the appearance of 841 and 1220 cm^{-1} bands at different temperatures, respectively. It clearly shows that the window between the critical flow rate to induce 1220 and 841 cm^{-1} bands increases with the increase in temperature. In other words, a stronger flow rate is required to induce the formation of longer helices, especially at high temperatures.

The flow rate window in Figure 4 guided us to investigate the structure evolution after shear. We focus on three different situations. (i) Both 841 and 1220 cm^{-1} bands do not appear immediately just after shear, whereas the 841 cm^{-1} band occurs after certain induction time. (ii) The 841 cm^{-1} band appears immediately after shear, whereas the 1220 cm^{-1} band does not occur even after waiting for a relatively long time. (iii) The 841 cm^{-1} band appears immediately after shear, whereas the 1220 cm^{-1} band occurs after a short induction time. These three cases are described in the following. Note the further extension of the waiting time after the cessation of shear; all conformational bands will increase and lead to the occurrence of crystallization, provided that 841 cm^{-1} bands can be induced.

Figure 5a,b gives differential spectra at 170 °C after being subjected to shear with a flow rate of 180 mm^3/s. The long helices with monomer numbers of 12 and 14, represented by 841 and 1220 cm^{-1} bands, do not appear immediately after shear. It takes about 2 min for the 841 cm^{-1} band to be clearly visible, whereas no signal of 1220 cm^{-1} band is observed after 100 min. A longer induction period (about 20 min) is observed at 171 °C for the 841 cm^{-1} band. However, Figure 5c shows that the intensities of 998 and 1100 cm^{-1} bands and so on are sharply increased by shear, which decrease after the cessation of shear. This indicates that the contents of the short helices are increased by shear, but helices no longer than those in the original melt were induced just after the shear. The intensity evolutions and the absence of the 1220 cm^{-1} band indicates that under this condition the nucleation and growth of long helices occurs without the onset of crystallization.

Imposing the shear flow at low temperature, the 841 cm^{-1} band can be observed immediately after the cessation of shear. Figure 6a,b gives the differential spectra at 160 °C after being subjected to shear with a flow rate of 45 mm^3/s. Although it is rather weak, the 841 cm^{-1} band can be clearly distinguished just

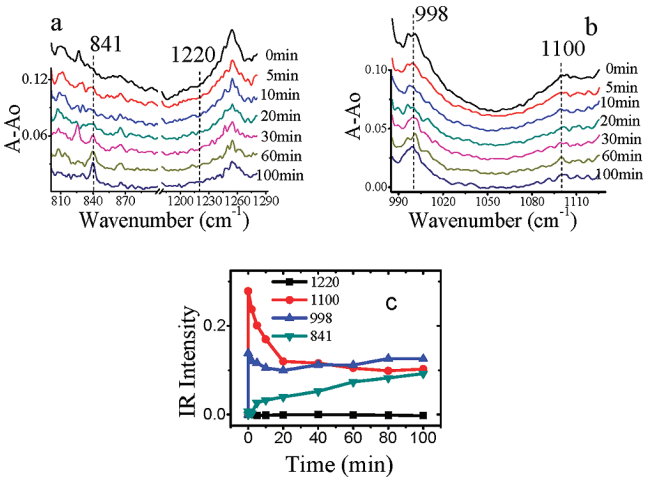

Figure 5. (a,b) IR differential spectra at different times after the cessation of shear with a shear flow rate of 180 mm^3/s at 170 °C. (c) IR intensities of 1220, 1100, 998, and 841 cm^{-1} bands versus time after the cessation of shear.

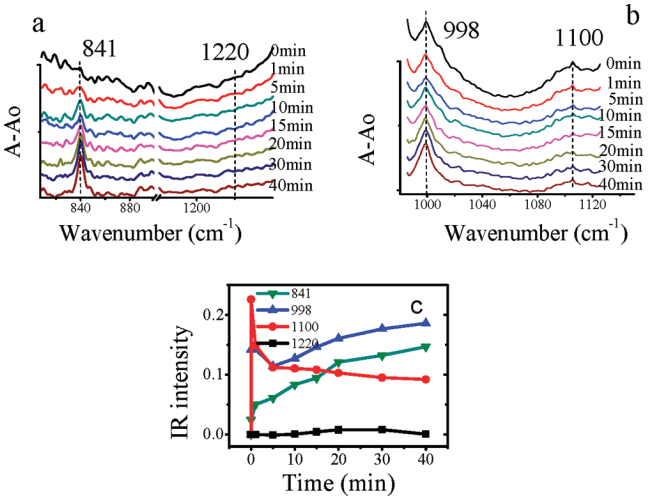

Figure 6. (a,b) IR differential spectra at different times after the cessation of shear with a shear flow rate of 45 mm^3/s at 160 °C. (c) IR intensities of 1220, 1100, 998, and 841 cm^{-1} bands versus time after the cessation of shear.

after shear, whose intensity increases monotonically with time. (See Figure 6c.) The intensity of the 841 cm^{-1} band increases sharply in the first stage, which is followed by a slow growth process. The 1220 cm^{-1} band does not appear after 40 min, indicating that crystallization has not yet occurred. Note that when the waiting time is further extended, the 1220 cm^{-1} band will appear. A sharp increase in intensities is also induced on the bands corresponding to short helices. However, after the cessation of shear, different intensity evolution processes are observed on different bands of the short helices. The 998 cm^{-1} band, corresponding to helices of 10 monomers, shows a sharp decrease first, which is followed by an increase in the later stage. The 1100 cm^{-1} band representing helices of about six monomers decreases monotonically in the time frame we recorded.

By further decreasing the temperature, it is possible to induce the occurrence of crystallization in a relatively short time. Figure 7a,b gives the differential spectra of iPP at 150 °C after being imposed by shear with a flow rate of 18 mm^3/s. The 841 cm^{-1} band appears immediately after shear, whereas an induction period of about 3 min is taken for the 1220 cm^{-1} band to be observable. As shown in Figure 7c,d, the intensities of all

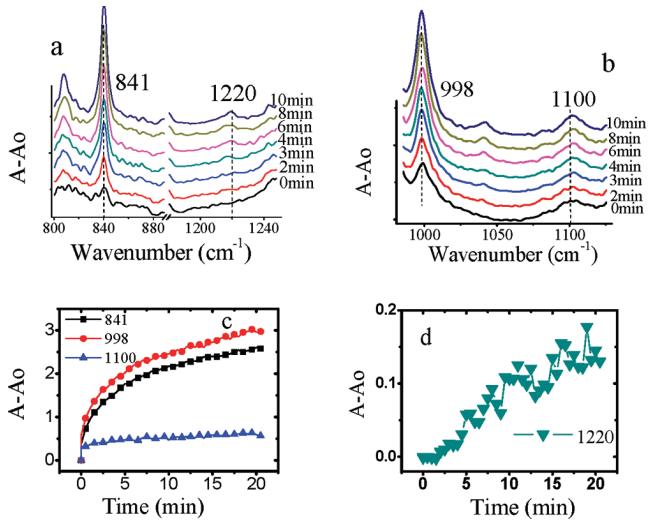

Figure 7. (a,b) IR differential spectra at different times after shear with a shear flow rate of 18 mm^3/s at 150 °C. (c,d) IR intensities of 1100, 998, 841, and 1220 cm^{-1} bands versus time after the cessation of shear.

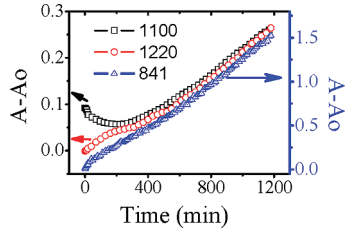

Figure 8. IR intensity evolution of 841, 1100, and 1220 cm^{-1} bands after the cessation of shear at 165 °C with a shear low rate of 90 mm^3/s.

conformational bands increase monotonically, and no relaxation process occurs after the cessation of shear.

By imposing strong shear flow at temperatures up to 171 °C, the intensity of the 841 cm^{-1} band is observed to increase continuously, and the 1220 cm^{-1} band will also appear after a relatively long period of waiting time. Then, all conformational bands increase with time, which demonstrates the occurrence of crystallization. Figure 8 shows the IR intensity evolution of 841, 1100, and 1220 cm^{-1} bands after shear at 165 °C with a flow rate of 90 mm^3/s. It can be found that there are two stages that are divided by the time of about 400 min. From 0 to 400 min after shear, the growth rate of the peak intensities of the 841 and 1220 cm^{-1} bands decreases sharply and reaches the smallest value at about 400 min after shear, whereas the peak intensity of the 1100 cm^{-1} band keeps decreasing during this period. Starting from 400 min, all peak intensities of 841, 998, 1220, and 1100 cm^{-1} bands begin to increase again, which indicates the completion of the induction period for crystallization.

To check the stability of the structures along with the waiting time after shear, we did the heating scan after waiting for different times after the cessation of shear. Figure 9a shows the intensity evolution of the 841 cm^{-1} band of the sheared samples during the heating scan with a rate of 1 °C/min, which were sheared with a flow rate of 75 mm^3/s at 165 °C with different waiting times after the shear. Note that at this temperature without imposing shear, the 841 cm^{-1} band did not appear after waiting for 24 h. The completely disappearing temperature during heating is plotted versus the waiting time in Figure 9b, which shows that the final melting temperature of the helices represented by the 841 cm^{-1} band increases with the waiting time in the first 100 min. The melting temperature reaches a plateau after about 200 min, which may indicate the completion of the perfection or transition process.

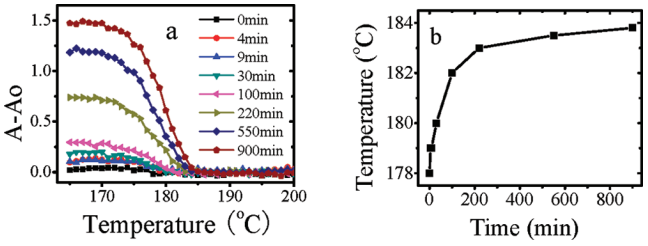

Figure 9. (a) Intensity evolution of 841 cm^{-1} bands during heating with a rate of 1 °C/min after waiting different amounts of time after the cessation of shear with a shear flow rate of 75 mm^3/s at 165 °C. (b) Complete disappearing temperature of 841 cm^{-1} versus waiting time.

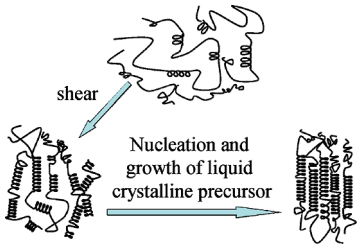

Figure 10. Schematic picture for the formation of flow-induced precursor.

Discussion

On the basis of the above experiments, a straightforward conclusion can be safely drawn that long helices with a monomer number of 12 can be induced by shear before the onset of crystallization, which does not exist in the melt under quiescent conditions. This conclusion further confirmed our early idea of flow-induced conformational ordering or coil−helix transition. Therefore, flow field provides the possibility for the formation of precursor, which has a "partial ordered" structure.

Unlike the short helices with monomer numbers smaller than 12, no relaxation is observed on the long helices at the temperatures we studied in this work. Similar to that at high temperatures,[55,56] 998 and 1100 cm^{-1} bands follow a relaxation process just after the cessation of shear at temperatures around the melting temperature. Irrespective of whether 841 cm^{-1} appears immediately after shear or after a certain induction period, its intensity increases monotonically after the cessation of shear. At 170 °C, the induction period is required for the 841 cm^{-1} band or helices with 12 monomers to occur, which clearly demonstrates that a nucleation and growth process is undertaken by the long helices. The same nucleation and growth process is expected to be followed at low temperature, although no induction period is detected, which can be attributed to low nucleation barrier at low temperature. By comparing the intensity evolutions of the 841 cm^{-1} band with the 998 and 1100 cm^{-1} bands in Figures 5 and 6 in the fist stage after the cessation of shear, we notice that the growth of long helices is accompanied by a reduction of short helices. The reduction of short helices may be partially due to the relaxation back to coil like at high temperatures; the nucleation and growth of long helices may consume some short helices, which seems to be reasonable in terms of thermodynamic origin as well as kinetic pathway.

The experimental results provide direct evidence of the nucleation and growth process for the formation of long helices. To accept this physical picture requires us to solve two issues: (i) Individually isolated long helices with 12 monomers are not stable in the melt. Without coupling to intermolecular ordering, the long helices should be less stable than the short ones. However, 998 and 1100 cm^{-1} bands, corresponding to short helices, undergo a reduction process after shear, whereas the 841 cm^{-1} band, representing helices with 12 monomers, continuously grows. This clearly indicates that helices with 12 monomers are more stable than the shorter ones. The shear-induced coil−helix transition and subsequent relaxation can be explained by the theory on stretched single chain or network because the content and length of helices are directly determined by the end-to-end distance of chains.[48,50,65−67] However, the theory cannot account for the growth of long helices after the cessation of shear. According to the theory, the end-to-end distance should relax back to Gaussian configuration, and long helices should disappear instead of growing. (ii) Coil−helix transition is not a thermodynamic phase transition if no other transition couples to this process. To meet these two challenges, the only solution is the coupling between intramolecular and intermolecular orderings such as positional or orientational orderings. After shearing at high temperatures, the 1220 cm^{-1} band does not appear in the first stage, which indicates that no crystallization occurs because crystals with thickness of <3 nm cannot form at these temperatures. This conclusion is also supported by the intensity evolution of all conformational bands. Therefore, during this process, positional order due to crystallization can be excluded. Coupling between conformational and orientational orderings seems to be a reasonable answer, which may lead to an isotropic−nematic phase transition. Theories of flexible-chain polymers show that rigidity induced by a coil−helix transition could provide the necessary stiffness to meet the conditions of the isotropic−nematic transition.[68,69] Many examples can be found in biopolymers such as DNA and proteins in which hydrogen bonds stabilize the helices.[70] The nucleation and growth process of the long helices can be exactly fitted in this frame.

Following Doi−Edwards' theory, the critical persistence length, l_p, for an isotropic−nematic transition can be calculated from the following formula[71−75]

$$l_p = \frac{4.19M_0}{bl_0\rho N_A} \quad (1)$$

In this equation, b represents the diameter of a polymer segment, ρ is the density, N_A is Avogadro's number, and M_0 and l_0 are the mass and the length of a monomer, respectively. For the iPP melt, $M_0 = 42$ g/mol, $b = 0.665$ nm, $l_0 = 0.217$ nm, and $\rho = 0.85$ g/cm^3. By inserting these values into eq 1, we find $l_p \approx 2.4$ nm, which is for a 3/1 helix equivalent to about 11 monomers.[62] Therefore, helices with 12 monomers meet the requirement for the isotropic−liquid-crystal transition. This leads to a reasonable conclusion that the nucleation and growth process of the long helices is actually the isotropic−liquid-crystal transition process, which is a real thermodynamic phase transition. Then, the flow-induced precursor may be a liquid crystal phase. This conclusion is in line with the estimation of the stability of the mesophase of iPP, which may have an equilibrium melting temperature that is much higher than that of crystal.

On the basis of the experimental data and discussion above, we reach a schematic picture for the formation of the flow-induced precursor. (See Figure 10.) Determined by the flow field and temperature, long helices with 12 monomers can be induced immediately after shear or appear after a certain induction period. As soon as the local concentration of long helices reaches the critical concentration, the isotropic−liquid-crystal phase transition will occur, which follows a nucleation and growth process. If the temperature allows the nucleation and growth of crystal to occur, then the liquid crystalline precursor will transform into crystal and initiate the growth process. The fast growth of the 841 cm^{-1} band in Figures 5, 6, and 8 and the increase in melting temperature of the structure represented by the 841 cm^{-1} band along with waiting time (Figure 9) indicate that the

precursor undergoes a perfection process under these conditions. With a strong flow field and large supercooling like that in Figure 2b and that reported by Balzano et al., the liquid crystalline precursor may not be the necessary step, and flow-induced crystalline nuclei can be directly induced.

The intensity evolution of long and short helices in this work and our early data are beautifully supporting: (i) Doi−Edwards' theory, (ii) theories on the coupling between coil−helix transition and isotropic−nematic transition, and (iii) our current model for flow-induced precursor. Helices with 10 or 6 monomers always show a reduction process after shear because they are too short to couple to isotropic−liquid-crystal transition. Therefore, without coupling to intermolecular ordering, they are unstable and either relax back to the coil or grow to be the long helices. However, long helices with 12 monomers meet the requirement of isotropic−liquid-crystal transition and are stabilized by the intermolecular ordering. This is perfectly consistent with our experimental data that no reduction of these long helices is observed after shear. After the nucleation of the liquid crystal phase, helices with 10 monomers can be incorporated into the liquid crystal phase, whereas the shorter ones can not because of the large gap for fulfilling the requirement of liquid crystalline ordering. This is why we observed an increase in the 998 cm^{-1} band in the later stage, whereas no increases in the absorption bands corresponding to shorter helices occur before crystallization.

Conclusions

At temperatures around the melting point of isotactic polypropylene, in situ FTIR study coupled to an extrusion slit die shows that helices with monomer numbers up to 12 and 14 can be induced by shear. A window of shear strength exists to induce helices with different lengths, which increases with temperature. After the cessation of shear, the intensity evolution of different conformational bands is obviously different. The 841 cm^{-1} band increases sharply in the first stage, which is followed by a slow growth process, whereas a reduction of shorter helices is observed after the cessation of shear. A heating scan on the samples of different waiting times after shear revealed that the final disappearance temperature of the 841 cm^{-1} band increases with the waiting time. The intensity evolutions of the long and short helical bands suggest that a coupling between the coil−helix transition and the intermolecular ordering occurs with helices with a length of 12 monomers, which may lead to an isotropic−liquid-crystal transition. Therefore the flow-induced precursor is a liquid crystal phase. After the cessation of shear, the sharp increase in the 841 cm^{-1} band and the stability of the long helices versus waiting time indicate that the precursor undergoes a perfection process, which eventually transforms into crystal and initiates further crystal growth.

Acknowledgment. This work is supported by the National Natural Science Foundation of China (50503015, 20774091), one hundred talent scientist fund, and the 'NCET' program of the Minister of Education. The research is also partially supported by the Opening Project of the State Key Laboratory of Polymer Materials Engineering (Sichuan University).

References and Notes

(1) Cates, M. E.; Mcleish, T. C. B.; Marrucci, G. *Europhys. Lett.* **1993**, *21*, 451–456.
(2) Nakatani, A. I.; Dadmun, M. D. *Flow-Induced Structure in Polymer*; American Chemical Society: Washington, DC, 1995.
(3) Li, L. B.; De Jeu, W. H. *Adv. Polym. Sci.* **2005**, *181*, 75–120.
(4) Somani, R. H.; Yang, L.; Zhu, L.; Hsiao, B. S. *Polymer* **2005**, *46*, 8587–8623.
(5) Eder, G.; Janeschitz-Kriegl, H.; Krobath, G. *Prog. Colloid Polym. Sci.* **1989**, *80*, 1–7.
(6) Kume, T.; Hattori, T.; Hashimoto, T. *Macromolecules* **1997**, *30*, 427–434.
(7) Onuki, A. *J. Phys.: Condens. Matter* **1997**, *9*, 6119–6157.
(8) Jay, F.; Haudin, J. M.; Monasse, B. *J. Mater. Sci.* **1999**, *34*, 2089–2102.
(9) Pogodina, N. V.; Siddiquee, S. K.; Van Egmond, J. W.; Winter, H. H. *Macromolecules* **1999**, *32*, 1167–1174.
(10) Hu, W. B.; Fenkel, D.; Mathot, V. B. F. *Macromolecules* **2002**, *35*, 7172–7174.
(11) Kornfield, J. A.; Kumaraswamy, G.; Issaian, A. M. *Ind. Eng. Chem. Res.* **2002**, *41*, 6383–6392.
(12) Janeschitz-Kriegl, H.; Ratajski, E.; Stablbauer, M. *Rheol. Acta* **2003**, *42*, 355–364.
(13) Muthukumar, M. *Adv. Polym. Sci.* **2005**, *191*, 241–274.
(14) Boukany, P. E.; Wang, S. Q. *Macromolecules* **2008**, *41*, 1455–1464.
(15) Kumaraswamy, G.; Verma, R. K.; Issaian, A. M.; Wang, P.; Kornfield, J. A.; Yeh, F.; Hsiao, B. S.; Olley, R. H. *Polymer* **2000**, *41*, 8931–8940.
(16) Ning, N. Y.; Luo, F.; Wang, K.; Zhang, Q.; Chen, F.; Du, R. N.; An, C. Y.; Pan, B. F.; Fu, Q. *J. Phys. Chem. B* **2008**, *112*, 14140–14148.
(17) Martins, J. A.; Zhang, W. D.; Brito, A. M. *Macromolecules* **2006**, *39*, 7626–7634.
(18) Fall, A.; Huang, N.; Bertrand, F.; Ovarlez, G.; Bonn, D. *Phys. Rev. Lett.* **2008**, *100*, 018301.
(19) Zhao, B. J.; Li, X. Y.; Huang, Y. J.; Cong, Y. H.; Ma, Z.; Shao, C. G.; An, H. N.; Yan, T. Z.; Li, L. B. *Macromolecules* **2009**, *42*, 1428–1432.
(20) Keum, J. K.; Zuo, F.; Hsiao, B. S. *Macromolecules* **2008**, *41*, 4766–4776.
(21) Kimata, S.; Sakurai, T.; Nozue, Y.; Kasahara, T.; Yamaguchi, N.; Karino, T.; Shibayama, M.; Kornfield, J. A. *Science* **2007**, *316*, 1014–1017.
(22) Ogino, Y.; Fukushima, H.; Takahashi, N.; Matsuba, G.; Nishida, K.; Kanaya, T. *Macromolecules* **2006**, *39*, 7617–7625.
(23) Gutiérrez, M. C. G.; Alfonso, G. C.; Riekel, C.; Azzurri, F. *Macromolecules* **2004**, *37*, 478–485.
(24) Kanaya, T.; Matsuba, G.; Ogino, Y.; Nishida, K.; Shimizu, H. M.; Shinohara, T.; Oku, T.; Suzuki, J.; Otomo, T. *Macromolecules* **2007**, *40*, 3650–3654.
(25) Wang, M. X.; Hu, W. B.; Ma, Y.; Ma, Y. Q. *Macromolecules* **2005**, *38*, 2806–2812.
(26) Balzano, L.; Kukalyekar, N.; Rastogi, S.; Peters, G. W. M.; Chadwick, J. C. *Phys. Rev. Lett.* **2008**, *100*, 048302.
(27) Keum, J. K.; Somani, R. H.; Zuo, F.; Burger, C.; Sics, I.; Hsiao, B. C.; Chen, H. Y.; Kolb, R.; Lue, C. T. *Macromolecules* **2005**, *38*, 5128–5136.
(28) Dikovsky, D.; Marom, G.; Avila-Orta, C. A.; Somani, R. H.; Hsiao, B. S. *Polymer* **2005**, *46*, 3096–3104.
(29) Somani, R. H.; Yang, L.; Hsiao, B. S.; Agarwal, P. K.; Fruitwala, H. A.; Tsou, A. H. *Macromolecules* **2002**, *35*, 9096–9104.
(30) Somani, R. H.; Hsiao, B. S.; Nogales, A.; Srinivas, S.; Tsou, A. H.; Sics, I.; Balta -Calleja, F. J.; Ezquerra, T. A. *Macromolecules* **2000**, *33*, 9385–9394.
(31) Somani, R. H.; Sics, I.; Hsiao, B. S. *J. Polym. Sci., Part B: Polym. Phys.* **2006**, *44*, 3553–3570.
(32) Yang, L.; Somani, R. H.; Sics, I.; Hsiao, B. S.; Kolb, R.; Lohse, D. *J. Phys.: Condens. Matter* **2006**, *18*, S2421–S2436.
(33) Heeley, E. L.; Fernyhough, C. M.; Graham, R. S.; Olmsted, P. D.; Inkson, N. J.; Embery, J.; Groves, D. J.; McLeish, T. C. B.; Morgovan, A. C.; Meneau, F.; Bras, W.; Ryan, A. J. *Macromolecules* **2006**, *39*, 5058–5071.
(34) Matsuba, G.; Sakamoto, S.; Ogino, Y.; Nishida, K.; Kanaya, T. *Macromolecules* **2007**, *40*, 7270–7275.
(35) Murase, H.; Kume, T.; Hashimoto, T.; Ohta, Y. *Macromolecules* **2005**, *38*, 6656–6665.
(36) Murase, H.; Kume, T.; Hashimoto, T.; Ohta, Y.; Mizukami, T. *Macromolecules* **1995**, *28*, 7724–7729.
(37) Pogodina, N. V.; Lavrenko, V. P.; Srinivas, S.; Winter, H. H. *Polymer* **2001**, *42*, 9031–9043.
(38) Kumaraswamy, G.; Issaian, A. M.; Kornfield, J. A. *Macromolecules* **1999**, *32*, 7537–7547.
(39) Fukushima, H.; Ogino, Y.; Matsuba, G.; Nishida, K.; Kanaya, T. *Polymer* **2005**, *46*, 1878–1885.
(40) Chai, C. K.; Dixon, N. M.; Gerrard, D. L.; Reed, W. *Polymer* **1995**, *36*, 661–663.
(41) Azzurri, F.; Alfonso, G. C. *Macromolecules* **2005**, *38*, 1723–1728.
(42) Azzurri, F.; Alfonso, G. C. *Macromolecules* **2008**, *41*, 1377–1383.

(43) Auriemma, F.; De Rosa, C.; Corradini, P. *Adv. Polym. Sci.* **2005**, *181*, 1–74.
(44) Bermejo, F. J.; Criado, A.; Fayos, R.; Fernandez, P, R.; Fischer, H. E.; Suard, E.; Guelylah, A.; Zuniga, J. *Phys. Rev. B* **1997**, *56*, 11536–11545.
(45) Strobl, G. *Eur. Phys. J. E* **2000**, *3*, 165–183.
(46) Matsuba, G.; Kaji, K.; Nishida, K.; Kanaya, T.; Imai, M. *Macromolecules* **1999**, *32*, 8932–8937.
(47) Konishi, T.; Nishida, K.; Kanaya, T. *Macromolecules* **2006**, *39*, 8035–8040.
(48) Courty, S.; Gornall, J. L.; Terentjev, E. M. *Proc. Natl. Acad. Sci. U. S.A.* **2005**, *102*, 13457–13460.
(49) Courty, S.; Gornall, J. L.; Terentjev, E. M. *Biophys. J.* **2006**, *90*, 1019–1027.
(50) Tanaka, F. *Macromolecules* **2000**, *33*, 4249–4263.
(51) Painter, P. C.; Coleman, M. M.; Koening, J. L. *The Theory of Vibrational Spectroscopy and Its Application to Polymeric Materials*; John Wiley & Sons: New York, 1982.
(52) Hollas, J. H. *Mordern Spectroscopy*, 4th ed.; John Wiley & Sons: West Sussex, U.K., 2004; p 137.
(53) Snyder, R. G.; Schachtschneider, J. H. *Spectrochim. Acta* **1964**, *20*, 853–869.
(54) Zhu, X. Y.; Yan, D. Y.; Yao, H. X.; Zhu, P. F. *Macromol. Rapid Commun.* **2000**, *21*, 354–357.
(55) An, H. N.; Zhao, B. J.; Ma, Z.; Shao, C. G.; Wang, X.; Fang, Y. P.; Li, L. B.; Li, Z, M. *Macromolecules* **2007**, *40*, 4740–4743.
(56) An, H. N.; Li, X. Y.; Geng, Y.; Wang, Y. L.; Wang, X.; Li, L. B.; Li, Z. M.; Yang, C. L. *J. Phys. Chem. B* **2008**, *112*, 12256–12262.
(57) Suter, U. W.; Flory, P, J. *Macromolecules* **1975**, *8*, 765–776.
(58) Tonelli, A. E. *Macromolecules* **1972**, *5*, 563–566.
(59) Zerbi, G.; Ciampelli, F.; Zamboni, V. *J. Polym. Sci.* **1963**, *C7*, 141–151.
(60) Kissin, Y. V.; Tsvetkova, V. I.; Chirkov, N. M. *Eur. Polym. J.* **1972**, *8*, 529–546.
(61) Miyamoto, T.; Inagaki, H. *J. Polym. Sci., Part A-2* **1969**, *7*, 963–981.
(62) Zhu, X. Y.; Yan, D. Y.; Fang, Y. P. *J. Phys. Chem. B* **2001**, *105*, 12461–12463.
(63) Budevska, B. O.; Manning, C. J.; Griffiths, P. R.; Roginski, R. T. *Appl. Spectrosc.* **1993**, *47*, 1843–1851.
(64) Balzano, L.; Rastogi, S.; Peters, G. W. M. *Macromolecules* **2009**, *42*, 2088–2092.
(65) Buhot, A.; Halperin, A. *Phys. Rev. Lett.* **2000**, *84*, 2160–2163.
(66) Buhot, A.; Halperin, A. *Macromolecules* **2002**, *35*, 3238–3252.
(67) Tamashiro, M. N.; Pincus, P. *Phys. Rev. E* **2001**, *63*, 021909.
(68) Matheson, R.; Flory, P. J. *J. Phys. Chem.* **1984**, *88*, 6606–6612.
(69) De Gennes, P. G.; Pincus, P. *Polym. Prepr.* **1977**, *18*, 161–166.
(70) Plotkin, S. S.; Onuchic, J. N. *Q. Rev. Biophys.* **2002**, *35*, 111–167.
(71) Matsuba, G.; Kaji, K.; Nishida, K. *Polym. J.* **1999**, *31*, 722–727.
(72) Flory, P. J. *Proc. R. Soc. London, Ser. A* **1956**, *234*, 60–73.
(73) Shimada, T.; Doi, M.; Okano, K. *J. Chem. Phys.* **1988**, *88*, 2815–2821.
(74) Doi, M.; Shimada, T.; Okano, K. *J. Chem. Phys.* **1988**, *88*, 4070–4075.
(75) Doi, M.; Edwards, S. F. *The Theory of Polymer Dynamics*; Clarendon: Oxford U.K., 1986.